PERGAMON

International Journal of Solids and Structures 38 (2001) 9525–9544

INTERNATIONAL JOURNAL OF SOLIDS and STRUCTURES

www.elsevier.com/locate/ijsolstr

Finite element modelling of orthotropic material behaviour in pneumatic membranes

S. Reese [a,*], T. Raible [b], P. Wriggers [b]

[a] *Institute of Mechanics, Ruhr University Bochum, D-44780 Bochum, Germany*

[b] *Institute for Structural and Computational Mechanics, University of Hannover, D-30167 Hannover, Germany*

Received 10 December 1999; in revised form 21 September 2000

Dedicated to Professor D. Gross on the occasion of his 60th birthday

Abstract

In this paper, we develop a model to describe the hyperelastic material behaviour of pneumatic membranes reinforced with roven–woven fibres. A generalized stored energy function is developed via a series of loading tests on a representative sample of this composite material. The exponents in the effective law are chosen so as to fulfil basic restrictions, discussed in the body of the paper, as well as to match certain experimental values. Numerical examples demonstrate the application of the approach to inflated rubber matrix materials, as well as laminated shells. © 2001 Elsevier Science Ltd. All rights reserved.

Keywords: Anisotropic elasticity; Wrinkling; Least square fit; Large deformations; Computer modelling

1. Introduction

Pneumatic membranes consist of multi-layered foils or fabric embedded in a matrix material. The fabric is usually made of polyester-, glass-, aramide- or carbon-fibres. Common coatings are rubber, PVC or Teflon. Frequently, such membrane structures serve as so-called "temporary" buildings (see Fig. 1). Due to their low weight, they are easy to transport and to install. Very popular are composites of polyester fibres and rubber coating, since these materials are relatively airtight and can be easily manufactured. The stability of structures as shown in Fig. 1 is maintained by a steady air pressure from the inside of the building. Pneumatic membranes undergo deformations of the moderate range, the stress strain behaviour is highly non-linear. Due to the fact that the fibres cannot carry any load in compression, we observe different material behaviour in tension and in compression.

Concerning anisotropic material models at finite strains, some research has been focussed on biomechanical problems. For instance, Holzapfel et al. (1996) investigated axisymmetric orthotropic blood vessels. Moderate deformations were also considered by Weiss et al. (1996), who modelled biological soft

* Corresponding author. Tel.: +49-234-32-25883; fax: +49-234-32-14488.
E-mail address: reese@nm.ruhr-uni-bochum.de (S. Reese).

0020-7683/01/$ - see front matter
PII: S0020-7683(01)00137-8

Fig. 1. Temporary building (inflated membrane structure).

tissues by means of an incompressible transversely isotropic law. A material law to describe the transversely isotropic material behaviour of rubber has been recently derived by Rüter and Stein (1999). Bonet and Burton (1998) developed orthotropic constitutive equations to simulate human leg impact problems. There is, however, still no material model available for the pneumatic membranes to be investigated in the present paper. One main difficulty is to develop a model which accounts for both tension and compression.

In Section 2, we present the basic equations and introduce the concept of structural tensors. Since experimental data for pneumatic membranes are poorly documented in the published literature, we set up a so-called "computer model" (Section 3). Running various tests with this "virtual" testing device, we obtain enough test data. A strain energy function is constructed upon the characteristics of these "experimental" results. In the following, the second Piola–Kirchhoff stresses and the material tensor are derived and the domain for the material parameters to achieve stable solutions is discussed. The formulation is further reduced to the case of a linear orthotropic material. In Section 5, the three-dimensional (3D) finite element formulation used in this work is discussed shortly. Section 6 provides two numerical examples which demonstrate the accuracy and efficiency of the present formulation.

2. Basic equations

We describe the deformation of a continuous body by means of the right Cauchy–Green tensor

$$\mathbf{C} = \mathbf{F}^T \cdot \mathbf{F}, \tag{1}$$

where $\mathbf{F}$ denotes the deformation gradient. A hyperelastic body is characterized by the existence of a scalar potential $W = \hat{W}(\mathbf{C})$, the stored energy function, from which the second Piola–Kirchhoff stress tensor $\mathbf{S}$ is obtained by

$$\mathbf{S} = 2\frac{\partial \hat{W}(\mathbf{C})}{\partial \mathbf{C}}. \tag{2}$$

In the case of orthotropic material behaviour, $\hat{W}(\mathbf{C})$ reduces to an isotropic function of $\mathbf{C}$ and the structural tensors

$$\mathbf{M}_1 = \mathbf{n}_1 \otimes \mathbf{n}_1 \quad \text{and} \quad \mathbf{M}_2 = \mathbf{n}_2 \otimes \mathbf{n}_2. \tag{3}$$

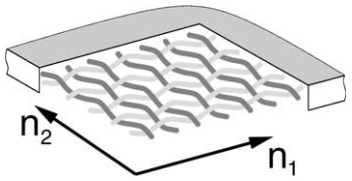

Fig. 2. Roven–woven structure with vectors $\mathbf{n}_i$ $(i = 1, 2)$.

See for a more detailed discussion the theoretical works of Boehler (1977, 1979), Liu (1982), Zhang and Rychlewski (1990) and Svendsen (1994). The vectors $\mathbf{n}_i$ $(i = 1, 2)$ are oriented parallel to the fibres in the membrane as indicated in Fig. 2.

The strain energy function W can be represented in dependence of the three invariants of $\mathbf{C}$,

$$I_1 := \operatorname{tr}\mathbf{C}, \qquad I_2 := \tfrac{1}{2}\big(I_1^2 - \operatorname{tr}(\mathbf{C}^2)\big), \qquad I_3 := \det \mathbf{C}, \tag{4}$$

and the first invariants of $\mathbf{C}\cdot\mathbf{M}_1$, $\mathbf{C}^2\cdot\mathbf{M}_1$, $\mathbf{C}\cdot\mathbf{M}_2$ and $\mathbf{C}^2\cdot\mathbf{M}_2$, respectively:

$$\begin{aligned} I_4 &:= \operatorname{tr}(\mathbf{C}\cdot\mathbf{M}_1) = \mathbf{C} : \mathbf{M}_1, \qquad & I_5 &:= \operatorname{tr}(\mathbf{C}^2\cdot\mathbf{M}_1) = \mathbf{C}^2 : \mathbf{M}_1, \\ I_6 &:= \operatorname{tr}(\mathbf{C}\cdot\mathbf{M}_2) = \mathbf{C} : \mathbf{M}_2, \qquad & I_7 &:= \operatorname{tr}(\mathbf{C}^2\cdot\mathbf{M}_2) = \mathbf{C}^2 : \mathbf{M}_2. \end{aligned} \tag{5}$$

Remark. Note that the relation

$$\sum_{j=1}^{3} \mathbf{n}_j \otimes \mathbf{n}_j = \mathbf{1}, \qquad \mathbf{n}_i \cdot \mathbf{n}_j = \delta_{ij}, \quad i, j = 1, 2, 3 \tag{6}$$

(δ_{ij} Kronecker delta) implies

$$\mathbf{M}_1 + \mathbf{M}_2 + \mathbf{M}_3 = \mathbf{1} \Rightarrow \mathbf{M}_3 = \mathbf{1} - \mathbf{M}_1 - \mathbf{M}_2, \tag{7}$$

i.e. $\mathbf{M}_3$ is linear dependent on $\mathbf{M}_1$ and $\mathbf{M}_2$. For this reason, $\mathbf{M}_3$ does not have to appear as independent variable. This corresponds to an alternative representation in standard text books like e.g. Jones (1999), where two orthogonal material property symmetry planes are suggested to define orthotropy. Symmetry will also exist for a third plane orthogonal to the others.

3. Computer experiments

Experimental data, although frequently found in the form of internal reports of companies, are poorly documented in the available literature. For this reason, we set up a "computer testing device" to obtain appropriate stress strain data. The material parameters of the orthotropic continuum mechanical model will then be fitted to these "experimental" results (see Section 4).

In Fig. 3, the computer model for the fibre reinforced membrane is shown. It consists of three-dimensional non-linear truss elements modelling the fibres and special low-order brick elements describing the rubber coating. The 3D element formulation will be discussed in Section 5.

To get a representative response, 10 fibres are placed in each direction. With this two phase approach, we are able to model the two constituents separately. For the rubber, the standard Neo-Hookean approach is used. Test results for polyester fibres in membrane fabrics can be found in Bidmon (1989).

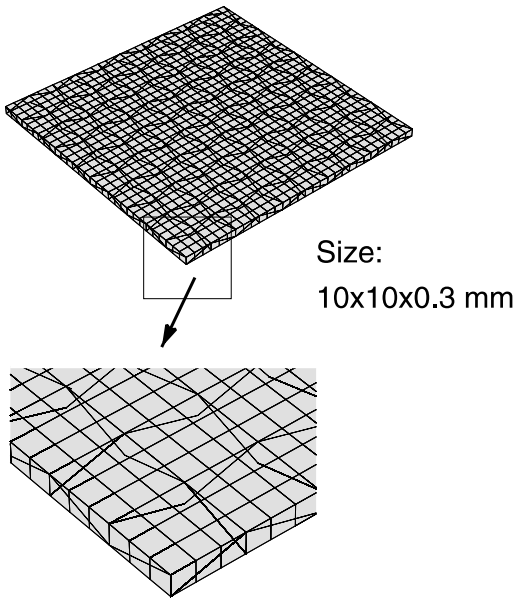

Fig. 3. Computer model.

3.1. Fibre model

Fig. 4 shows the experimental data for the fibres. The strain values are given in percent and refer to the linearized strain measure $\Delta L/L$ (L initial length of the test sample). The qualitative behaviour is somewhat rubber-like, although the characteristic S-shape is observed in the small strain range. Therefore, we implement an Ogden-type model (Ogden, 1972) into the truss element formulation which has the ability to capture S-shapes. The isotropic strain energy function

$$W_{\mathrm{OG}} = \sum_{r=1}^{n} \frac{\mu_r}{\alpha_r}\left(\lambda_1^{\alpha_r} + \lambda_2^{\alpha_r} + \lambda_3^{\alpha_r} - 3\right) + f(I_3), \tag{8}$$

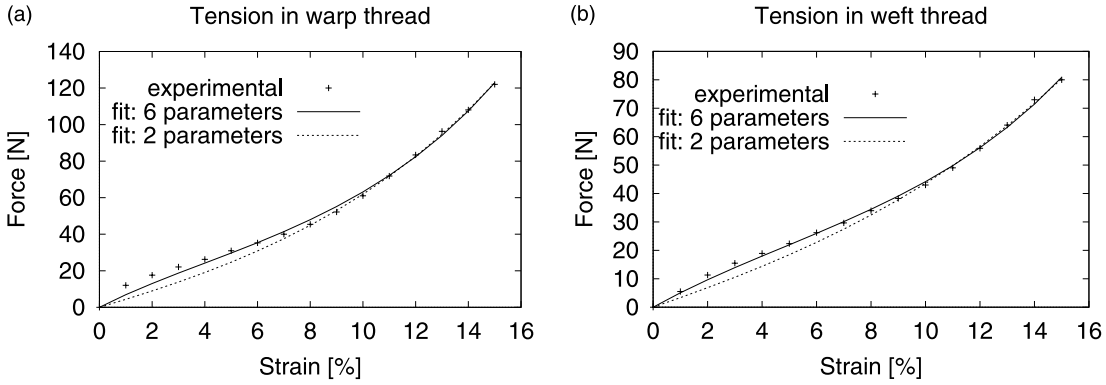

Fig. 4. Force–strain behaviour of fibres: (a) warp thread, (b) weft thread.

is given in terms of the principal stretches λ_i $(i = 1, 2, 3)$, i.e. the eigenvalues of the right stretch tensor $\mathbf{U} = \sqrt{\mathbf{C}}$. Moreover, we restrict ourselves here to a one-dimensional consideration. Then, using the assumption of incompressibility ($\lambda_1\lambda_2\lambda_3 = 1 \Rightarrow \lambda_2 = \lambda_3 = \sqrt{\lambda_1^{-1}} := \sqrt{\lambda^{-1}}$), Eq. (8) reduces to

$$W_{\mathrm{OG}} = \sum_{r=1}^{n} \frac{\mu_r}{\alpha_r}\left(\lambda^{\alpha_r} + 2\lambda^{-0.5\alpha_r} - 3\right), \tag{9}$$

and the force in the truss can be determined to be

$$F = A\frac{\partial W_{\mathrm{OG}}}{\partial \lambda} = \frac{A}{\lambda}\sum_{r=1}^{n} \mu_r\left(\lambda^{\alpha_r} - \lambda^{-0.5\alpha_r}\right), \tag{10}$$

where A denotes the initial area of the truss.

In order to use a standard (linear) least square fit, we set the exponents α_r equal to some reasonable number and compute only the "linear" parameters μ_r. This procedure is repeated for another choice of exponents, until a sufficiently accurate fit of the data is obtained. Material parameter sets were calculated for $n = 1$ (2 parameters) and $n = 3$ (6 parameters). The results are shown in Fig. 4. Note that the fibres in the 1- (warp) and 2- (weft) direction of the membrane possess different mechanical properties. In general good agreement is achieved for the six parameter sets. Two parameters are insufficient to model the characteristic S-curve in the small strain range. However, this deviation of the simpler model from the realistic behaviour is negligible, if one considers the computer model as a whole. Therefore, for simplicity, we work with the two parameter sets. A summary of the material parameters is given in Table 1.

3.2. Rubber coating

For the rubber coating we use the Neo-Hooke model

$$W_{\mathrm{NH}} = \frac{\mu}{2}(I_1 - 3) - \mu \ln\sqrt{I_3} + \frac{\Lambda}{4}\left(I_3 - 1 - 2\ln\sqrt{I_3}\right) \tag{11}$$

with the material parameters $\mu = 1.4$ N/mm^2 and $\Lambda = 500$ N/mm^2. So, the small strain stiffness of the fibres is about 700 times higher than that of the rubber material.

3.3. Numerical simulation

The "experimental" results are achieved by a simulation of various tests. The advantage of a "virtual" testing device is that enough independent test data can be provided easily. This is especially important, if the material behaves anisotropically, since in this case usually a quite large number of material parameters has to be determined. The results for uniaxial tension and various biaxial tests are plotted in Fig. 5. A plane

Table 1
Fibre material parameters

	Warp thread	Weft thread
$n = 1$:	$\mu = 174.16$ N/mm^2, $\alpha = 14.0$	$\mu = 169.20$ N/mm^2, $\alpha = 11.3$
$n = 3$:	$\mu_1 = 3.032$ N/mm^2, $\alpha_1 = 30.5$	$\mu_1 = 2.561$ N/mm^2, $\alpha_1 = 30.5$
	$\mu_2 = -9.362$ N/mm^2, $\alpha_2 = -26$	$\mu_2 = -52.865$ N/mm^2, $\alpha_2 = -21.5$
	$\mu_3 = -142.573$ N/mm^2, $\alpha_2 = -26.5$	$\mu_3 = -86.801$ N/mm^2, $\alpha_2 = -20.5$

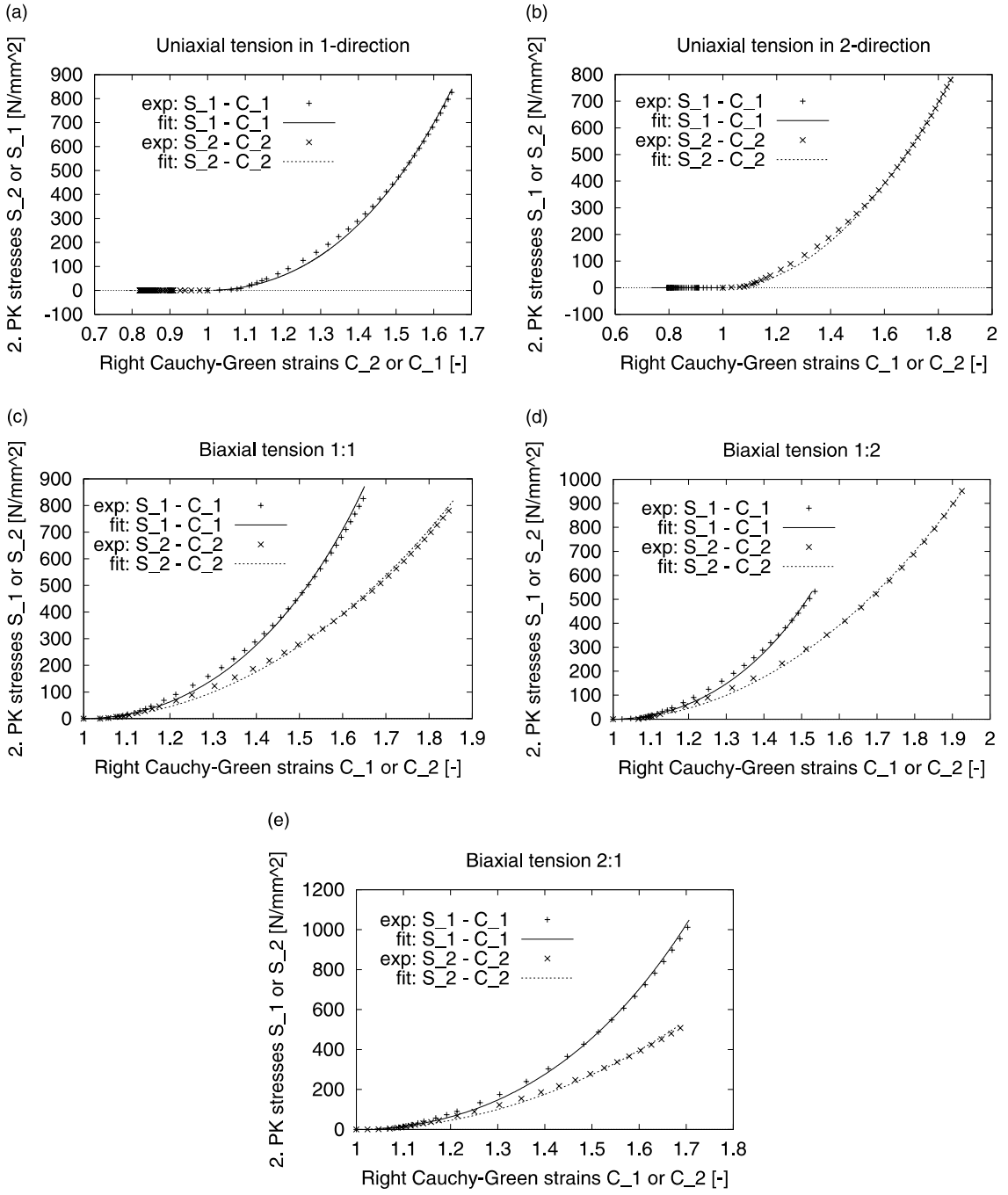

Fig. 5. S_i–C_i curves: (a) uniaxial tension (warp direction), (b) uniaxial tension (weft direction), (c) biaxial tension (1:1), (d) biaxial tension (1:2) and (e) biaxial tension (2:1).

stress state is assumed. The principal values of the second Piola–Kirchhoff stress S_i $(i = 1, 2)$ are computed by means of the equation

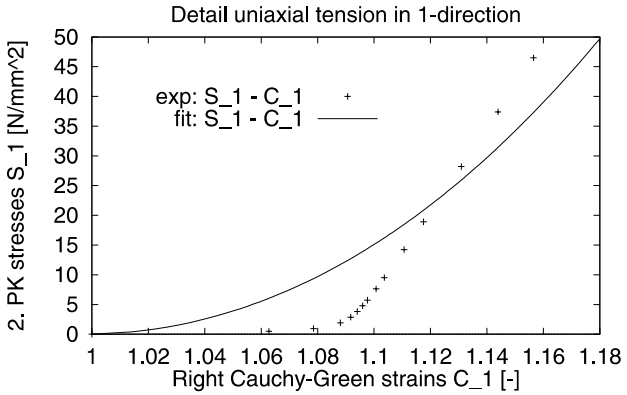

Fig. 6. Magnification of Fig. 5a.

$$S_i = \frac{F_i}{A_i}\frac{1}{\sqrt{C_i}}, \quad C_i = \lambda_i^2. \tag{12}$$

In the latter relation, F_i denotes the total reaction force in i-direction and A_i the initial cross-sectional area perpendicular to the cartesian coordinate X_i. It is given by the length of the test sample (10 mm) multiplied with the thickness (0.3 mm). The magnification of the first test in Fig. 6 shows an unexpected kink at 4.4% strain ($\hat{=}\ C_1 = 1.09$) which can be explained as follows.

Since the fibres are not fully extended in their initial configuration (solid line in Fig. 7), one can pull them in a stress-free state up to the point, where they are stretched straight. The strain at this time is easily calculated from comparing the initial length of the fibres ($L = 10.44$ mm) with the length of the test sample (10 mm). So, the stresses measured in the small strain regime are due to the interaction with the rubber matrix alone and therefore very small. Beyond this limit, the stress in the fibres increases rapidly (see Fig. 5) and the stress–strain relationship of the membrane is dominated by the behaviour of the fibres. In the direction of compression, the situation is in general similar to the small strain case. The fibres do not carry any load. Consequently, the stiffness of the structure in this direction as well as the bending stiffness is almost zero.

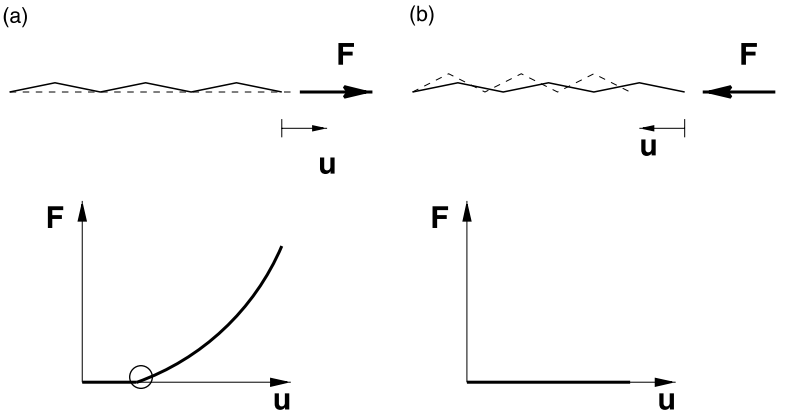

Fig. 7. Fibre behaviour: (a) tension and (b) compression.

4. Continuum mechanical model

The computer model did not only provide "experimental" data but let us also gain a deeper understanding of the membrane behaviour under different loading conditions. We must differentiate between three situations: (I) in the small strain regime, the fibres are not effective. The load is carried by the rubber matrix, i.e. the material behaves isotropically. (II) The compressive range, where the fibres are in general not effective. In many applications, however, compression in one direction means tension in the perpendicular direction. In this case, we observe transversely isotropic material behaviour. (III) For large tensile strains, the fibres determine the overall deformation behaviour of the membrane (orthotropic material behaviour). The influence of the rubber matrix then becomes negligible.

4.1. Strain energy function

In order to account for all three situations, the following choice for the strain energy function is appropriate:

$$W = \underbrace{\hat{W}_{\mathrm{NH}}(I_1, I_3)}_{\text{Neo-Hooke}} + \underbrace{\hat{W}^{+}_{\mathrm{iso}}(I_1, I_2)}_{\text{isotropic (+)}} + \underbrace{\hat{W}_{\mathrm{ani}}(I_4, I_5, I_6, I_7)}_{\text{orthotropic}}. \tag{13}$$

The Neo-Hookean part has already been given by Eq. (11). The additional term W^{+}_{iso}

$$W^{+}_{\mathrm{iso}} = K_1^{\mathrm{iso}}(I_1 - 3)^{\alpha_1} + K_2^{\mathrm{iso}}(I_2 - 3)^{\alpha_2} \tag{14}$$

is needed to model the extreme stiffening in the moderate and large deformation case. It is well-known that the Neo-Hooke model is not appropriate to display the increase of the stress in this range of deformation. With the last part

$$\begin{aligned} W_{\mathrm{ani}} = {} & K_1^{\mathrm{ani}\ 1}(I_4 - 1)^{\beta_1} + K_2^{\mathrm{ani}\ 1}(I_5 - 1)^{\beta_2} + K_1^{\mathrm{ani}\,2}(I_6 - 1)^{\gamma_1} + K_2^{\mathrm{ani}\ 2}(I_7 - 1)^{\gamma_2} \\ & + K^{\mathrm{coup}\,1}(I_1 - 3)^{\delta_1}(I_4 - 1)^{\delta_1} + K^{\mathrm{coup}\,2}(I_1 - 3)^{\delta_2}(I_6 - 1)^{\delta_2} + K^{\mathrm{coup\,ani}}(I_4 - 1)^{\xi}(I_6 - 1)^{\xi}, \end{aligned} \tag{15}$$

the orthotropic properties of the fabric are included in the model. Here, we have to take into account that the material behaves differently in tension and compression.

For this purpose, consider an arbitrary deformation $\mathbf{C} = C_{ij}\mathbf{n}_i \otimes \mathbf{n}_j$ (Einstein's summation convention is assumed to hold over repeated indices). The matrix $(M_1)_{ij}$ associated with the structural tensor $\mathbf{M}_1$ takes the form

$$(M_1)_{ij} = \begin{bmatrix} 1 & 0 & 0 \\ 0 & 0 & 0 \\ 0 & 0 & 0 \end{bmatrix}. \tag{16}$$

The quantities I_i $(i = 4, 5, 6, 7)$ are then determined according to Eq. (5) with $I_4 = C_{11}$, $I_5 = C_{11}^2 + C_{12}^2 + C_{31}^2$, $I_6 = C_{22}$ and $I_7 = C_{12}^2 + C_{22}^2 + C_{23}^2$. If $C_{11} > 1$ and $C_{22} < 1$, the fibres in warp direction are pulled and the fibres in weft direction are compressed. Consequently, the parameters in Eq. (15) must be chosen in such a way that transversely isotropic material behaviour with $\mathbf{M}_1 = \mathbf{M}$ as only structural tensor is obtained. The opposite case can be treated analogously. Compression in warp and weft direction should lead to purely isotropic behaviour. The requirements discussed in the above are incorporated into the model by implementing the relationships

$$
\begin{aligned}
K_i^{\text{ani}\,1} &= \bar{K}_i^{\text{ani}\,1}\mathsf{inv4}, \quad i = 1,2,\\
K_i^{\text{ani}\,2} &= \bar{K}_i^{\text{ani}\,2}\mathsf{inv6}, \quad i = 1,2,\\
K^{\text{coup}\,1} &= \bar{K}^{\text{coup}\,1}\mathsf{inv4},\\
K^{\text{coup}\,2} &= \bar{K}^{\text{coup}\,2}\mathsf{inv6},\\
K^{\text{coup ani}} &= \bar{K}^{\text{coup ani}}\mathsf{inv4}\ \mathsf{inv6}.
\end{aligned}
\tag{17}
$$

In these equations, $\mathsf{inv}i$ $(i = 4, 6)$ represents a short-hand notation for the expression

$$
\mathsf{inv}i = \begin{cases} \frac{1}{2}(1 + \operatorname{sign}(I_i - 1)) & \text{if } I_i - 1 \neq 0,\\ 0 & \text{if } I_i - 1 = 0. \end{cases}
\tag{18}
$$

Due to the fact that $\mathsf{inv}i$ is only different from zero (and positive) if $I_i - 1 > 0$ $(i = 4, 6)$ holds, the stress contributions associated with inv4 and inv6 are "switched-off" for the compression states $C_{11} < 1$ or $C_{22} < 1$, respectively.

$\bar{K}_i^{\text{ani}\,1}$, $\bar{K}_i^{\text{ani}\,2}$, $\bar{K}^{\text{coup}\,1}$, $\bar{K}^{\text{coup}\,2}$, $\bar{K}^{\text{coup ani}}$, β_i, γ_i, δ_i and ξ as well as μ (in W_{NH}), K_i^{iso} and α_i in W_{iso}^{+} $(i = 1, 2)$ are material constants which have to be fitted to the "experimental" results shown in Fig. 5. This fit is based on the assumption of incompressibility, such that the Lamé constant Λ remains here undetermined. The function $-\mu \ln\sqrt{I_3} + (\Lambda/4)(I_3 - 1 - 2\ln\sqrt{I_3})$ is then replaced by $-p(\sqrt{I_3} - 1)$, where p denotes the hydrostatic pressure. It is even easier to insert the incompressibility condition $C_3 = 1/C_1C_2$ directly and to derive S_1 and S_2 in the usual way. In the finite element calculation, Λ plays the role of a penalty parameter.

Thus, in its present state, the model includes 19 material parameters. Since we deal here with a highly non-linear problem, it is desirable to reduce this number further. In order to derive physically reasonable constitutive restrictions, we compute the second Piola–Kirchhoff stress tensor $\mathbf{S}$ and the material tensor

$$
\mathscr{L} = 4\frac{\partial^2 W}{\partial \mathbf{C}^2}
\tag{19}
$$

in what follows.

4.2. Second Piola–Kirchhoff stress tensor and material tensor

To calculate the second Piola–Kirchhoff stress tensor, the derivatives of I_i $(i = 1, 2, \ldots, 7)$ with respect to $\mathbf{C}$

$$
\frac{\partial I_1}{\partial \mathbf{C}} = \mathbf{1}, \qquad \frac{\partial I_2}{\partial \mathbf{C}} = I_1\mathbf{1} - \mathbf{C}, \qquad \frac{\partial I_3}{\partial \mathbf{C}} = I_3\mathbf{C}^{-1},
\tag{20}
$$

$$
\frac{\partial I_4}{\partial \mathbf{C}} = \mathbf{M}_1, \qquad \frac{\partial I_5}{\partial \mathbf{C}} = \mathbf{C}\cdot\mathbf{M}_1 + \mathbf{M}_1\cdot\mathbf{C},
\tag{21}
$$

$$
\frac{\partial I_6}{\partial \mathbf{C}} = \mathbf{M}_2, \qquad \frac{\partial I_7}{\partial \mathbf{C}} = \mathbf{C}\cdot\mathbf{M}_2 + \mathbf{M}_2\cdot\mathbf{C}
\tag{22}
$$

have to be calculated. Using Eq. (2) in combination with Eqs. (11), (14) and (15) leads to

$$
\mathbf{S}_{\text{NH}} = \mu(\mathbf{1} - \mathbf{C}^{-1}) + \frac{\Lambda}{2}(I_3 - 1)\mathbf{C}^{-1},
\tag{23}
$$

$$
\mathbf{S}_{\text{iso}}^{+} = 2\alpha_1 K_1^{\text{iso}}(I_1 - 3)^{\alpha_1 - 1}\mathbf{1} + 2\alpha_2 K_2^{\text{iso}}(I_2 - 3)^{\alpha_2 - 1}(I_1\mathbf{1} - \mathbf{C})
\tag{24}
$$

and

$$\begin{aligned}\mathbf{S}_{\text{ani}} &= 2\beta_1 K_1^{\text{ani}\,1}(I_4-1)^{\beta_1-1}\mathbf{M}_1 + 2\beta_2 K_2^{\text{ani}\,1}(I_5-1)^{\beta_2-1}(\mathbf{C}\cdot\mathbf{M}_1+\mathbf{M}_1\cdot\mathbf{C}) + 2\gamma_1 K_1^{\text{ani}\,2}(I_6-1)^{\gamma_1-1}\mathbf{M}_2 \\ &\quad + 2\gamma_2 K_2^{\text{ani}\,2}(I_7-1)^{\gamma_2-1}(\mathbf{C}\cdot\mathbf{M}_2+\mathbf{M}_2\cdot\mathbf{C}) + 2\delta_1 K^{\text{coup}\,1}\Big[(I_1-3)^{\delta_1-1}(I_4-1)^{\delta_1}\mathbf{1} \\ &\quad + (I_1-3)^{\delta_1}(I_4-1)^{\delta_1-1}\mathbf{M}_1\Big] + 2\delta_2 K^{\text{coup}\,2}\Big[(I_1-3)^{\delta_2-1}(I_6-1)^{\delta_2}\mathbf{1} + (I_1-3)^{\delta_2}(I_6-1)^{\delta_2-1}\mathbf{M}_2\Big] \\ &\quad + 2\xi K^{\text{coup ani}}\Big[(I_4-1)^{\xi-1}(I_6-1)^{\xi}\mathbf{M}_1 + (I_4-1)^{\xi}(I_6-1)^{\xi-1}\mathbf{M}_2\Big]. \end{aligned} \tag{25}$$

Further, we introduce the short-hand notations

$$\mathscr{D}_0 := -\frac{\partial \mathbf{C}^{-1}}{\partial \mathbf{C}}, \qquad \mathscr{D}_\alpha := (D_\alpha)_{ijkl}\mathbf{e}_i\otimes\mathbf{e}_j\otimes\mathbf{e}_k\otimes\mathbf{e}_l, \;\; \alpha = 1,2 \tag{26}$$

$$(\mathscr{D}_\alpha)_{ijkl} = \tfrac{1}{2}(\delta_{jk}(M_\alpha)_{il} + \delta_{ik}(M_\alpha)_{jl} + \delta_{il}(M_\alpha)_{jk} + \delta_{jl}(M_\alpha)_{ik}) \tag{27}$$

and $\mathscr{I}$ denotes the fourth-order identity tensor. This gives us

$$\mathscr{L}_{\text{NH}} = 2\mu\mathscr{D}_0 + \Lambda I_3\mathbf{C}^{-1}\otimes\mathbf{C}^{-1} - \Lambda(I_3-1)\mathscr{D}_0, \tag{28}$$

$$\begin{aligned}\mathscr{L}^{+}_{\text{iso}} &= 4\alpha_1(\alpha_1-1)K_1^{\text{iso}}(I_1-3)^{\alpha_1-2}\mathbf{1}\otimes\mathbf{1} + 4\alpha_2(\alpha_2-1)K_2^{\text{iso}}(I_2-3)^{\alpha_2-2}(I_1\mathbf{1}-\mathbf{C})\otimes(I_1\mathbf{1}-\mathbf{C}) \\ &\quad + 4\alpha_2 K_2^{\text{iso}}(I_2-3)^{\alpha_2-1}(\mathbf{1}\otimes\mathbf{1}-\mathscr{I}) \end{aligned} \tag{29}$$

and

$$\begin{aligned}\mathscr{L}_{\text{ani}} &= 4\beta_1(\beta_1-1)K_1^{\text{ani}\,1}(I_4-1)^{\beta_1-2}\mathbf{M}_1\otimes\mathbf{M}_1 + 4\beta_2(\beta_2-1)K_2^{\text{ani}\,1}(I_5-1)^{\beta_2-2}\frac{\partial I_5}{\partial\mathbf{C}}\otimes\frac{\partial I_5}{\partial\mathbf{C}} \\ &\quad + 4\beta_2 K_2^{\text{ani}\,1}(I_5-1)^{\beta_2-1}\mathscr{D}_1 + 4\gamma_1(\gamma_1-1)K_1^{\text{ani}\,2}(I_6-1)^{\gamma_1-2}\mathbf{M}_2\otimes\mathbf{M}_2 + 4\gamma_2(\gamma_2-1)K_2^{\text{ani}\,2}(I_7-1)^{\gamma_2-2} \\ &\quad \times\frac{\partial I_7}{\partial\mathbf{C}}\otimes\frac{\partial I_7}{\partial\mathbf{C}} + 4\gamma_2 K_2^{\text{ani}\,2}(I_7-1)^{\gamma_2-1}\mathscr{D}_2 + 4\delta_1 K^{\text{coup}\,1}\Big[(\delta_1-1)(I_1-3)^{\delta_1-2}(I_4-1)^{\delta_1}\mathbf{1}\otimes\mathbf{1} \\ &\quad + \delta_1(I_1-3)^{\delta_1-1}(I_4-1)^{\delta_1-1}(\mathbf{M}_1\otimes\mathbf{1}+\mathbf{1}\otimes\mathbf{M}_1) + (\delta_1-1)(I_1-3)^{\delta_1}(I_4-1)^{\delta_1-2}\mathbf{M}_1\otimes\mathbf{M}_1\Big] \\ &\quad + 4\delta_2 K^{\text{coup}\,2}\Big[(\delta_2-1)(I_1-3)^{\delta_2-2}(I_6-1)^{\delta_2}\mathbf{1}\otimes\mathbf{1} + \delta_2(I_1-3)^{\delta_2-1}(I_6-1)^{\delta_2-1} \\ &\quad \times(\mathbf{M}_2\otimes\mathbf{1}+\mathbf{1}\otimes\mathbf{M}_2) + (\delta_2-1)(I_1-3)^{\delta_2}(I_6-1)^{\delta_2-2}\mathbf{M}_2\otimes\mathbf{M}_2\Big] \\ &\quad + 4\xi K^{\text{coup ani}}\Big[(\xi-1)(I_4-1)^{\xi-2}(I_6-1)^{\xi}\mathbf{M}_1\otimes\mathbf{M}_1 + \xi(I_4-1)^{\xi-1}(I_6-1)^{\xi-1}(\mathbf{M}_2\otimes\mathbf{M}_1+\mathbf{M}_1\otimes\mathbf{M}_2) \\ &\quad + (\xi-1)(I_4-1)^{\xi}(I_6-1)^{\xi-2}\mathbf{M}_2\otimes\mathbf{M}_2\Big]. \end{aligned} \tag{30}$$

The expressions $I_i - 3$ $(i = 1,2)$ and $I_j - 1$ $(j = 5,7)$ might become negative whereas $I_4 - 1$ and $I_6 - 1$ are always positive. Therefore, the exponents α_i, β_2, γ_2 and δ_i $(i = 1,2)$ have to be positive integers and larger than 2 (i.e. $\geqslant 3$). Either $\mathbf{S}$ or $\mathscr{L}$ would contain undetermined terms otherwise. For simplicity, this requirement is applied to all exponents. The undeformed configuration ($\mathbf{C} = \mathbf{1}$) is then automatically stress-free.

Another important issue is the question of stability. Using the existence theorem of Ball (1977) we have to prove polyconvexity of the stored energy function (see also Marsden and Hughes (1983)). This yields the usual restrictions for the material parameters in W_{NH} ($\mu > 0$, $\Lambda > -2/3\mu$). In anisotropic elasticity, however, it is not clear how a polyconvex strain energy function should be constructed. Thus, in order to achieve stability, we follow here a more intuitive strategy by including the modifications

$$
\begin{aligned}
K_1^{\text{iso}} &= \bar{K}_1^{\text{iso}}\text{jnv1}, \quad i = 1,2,\\
K_2^{\text{iso}} &= \bar{K}_2^{\text{iso}}\text{jnv2}, \quad i = 1,2,\\
K_2^{\text{ani}\,1} &= \bar{K}_2^{\text{ani}\,1}\text{inv4}\,\text{inv5},\\
K_2^{\text{ani}\,2} &= \bar{K}_2^{\text{ani}\,2}\text{inv6}\,\text{inv7},\\
K^{\text{coup}\,1} &= \bar{K}^{\text{coup}\,1}\text{inv4}\,\text{jnv1},\\
K^{\text{coup}\,2} &= \bar{K}^{\text{coup}\,2}\text{inv6}\,\text{jnv1}
\end{aligned}
\tag{31}
$$

and the inequalities

$$
\bar{K}_i^{\text{iso}}, \bar{K}_i^{\text{ani}\,1}, \bar{K}_i^{\text{ani}\,2}, \bar{K}^{\text{coup}\,1}, \bar{K}^{\text{coup}\,2}, \bar{K}^{\text{coup ani}} \geqslant 0, \quad i = 1,2. \tag{32}
$$

jnv$i$ is determined by

$$
\text{jnv}i = \begin{cases} \frac{1}{2}(1 + \text{sign}(I_i - 3)) & \text{if } I_i - 3 \neq 0,\\ 0 & \text{if } I_3 - 1 = 0. \end{cases} \tag{33}
$$

Note that the small strain stiffness is practically only determined by the Neo-Hooke part of the model, because the other stress contributions are negligible in this strain range. Therefore, we are able to determine the shear modulus μ in advance to reduce the number of material parameters at least by one. The least square fit is then carried out in the same way as described in Section 3. The constitutive inequalities can be incorporated easily. It should be emphasized that we fit our model to the five experiments simultaneously. In this way, we obtain one set of parameters which shows a very good agreement for all five tests. Restricting the exponents to the range from 3 to 6, the following material parameters (continuum mechanical model) were computed (see Fig. 5):

$$
\begin{aligned}
&\mu = 5.808\ \text{N/mm}^2,\\
&K_1^{\text{iso}} = 1.145\ \text{N/mm}^2, && \alpha_1 = 4,\\
&K_2^{\text{iso}} = 0.318\ \text{N/mm}^2, && \alpha_2 = 6,\\
&K_1^{\text{ani}\,1} = 171.174\ \text{N/mm}^2, && \beta_1 = 3,\\
&K_2^{\text{ani}\,1} = 6.962\ \text{N/mm}^2, && \beta_2 = 3,\\
&K_1^{\text{ani}\,2} = 179.135\ \text{N/mm}^2, && \gamma_1 = 3,\\
&K_2^{\text{ani}\,2} = 0.00157\ \text{N/mm}^2, && \gamma_2 = 6,\\
&K^{\text{coup}\,1} = 0\ \text{N/mm}^2,\\
&K^{\text{coup}\,2} = 0\ \text{N/mm}^2,\\
&K^{\text{coup ani}} = 5.753\ \text{N/mm}^2, && \xi = 6.
\end{aligned}
\tag{34}
$$

Using the constitutive restrictions discussed in the above we were able to reduce the number of material parameters to 15. The parameters which enter the isotropic part of the model lie in the range of 0–10 N/mm^2. As expected, these constants describe mainly the stiffness of the rubber matrix. On the other hand, the "anisotropic" constants $K_1^{\text{ani}\,1}$ and $K_1^{\text{ani}\,2}$ are very close to the fibre stiffnesses. Since the anisotropic behaviour of the membrane is controlled by the stress state in the fibres, such a result is very satisfying from the physical point of view. Note again that the fibre stiffnesses are only effective in tension. The accuracy of the fit could be even improved by including exponents up to 8 or 10.

4.3. Shear tests

To validate the results at this stage, two simple shear tests (plane stress state) were performed. The calculations were carried out for the computer model (Section 3) and the continuum mechanical model (Section 4) using the material parameters given there. The boundary conditions for the test and the

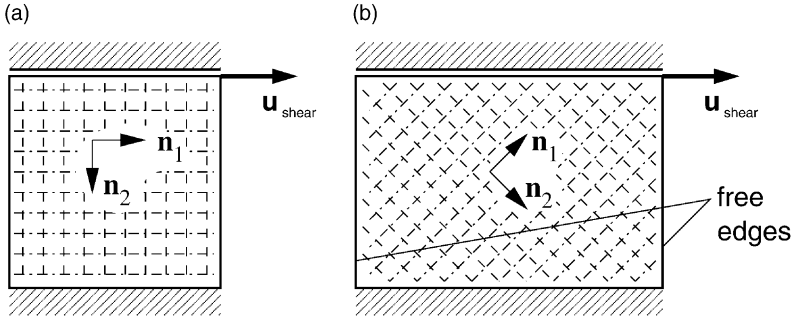

Fig. 8. Shear tests.

orientation of the fibres are shown in Fig. 8. The displacement perpendicular to the membrane plane is constrained on one side.

Two basic cases are selected: (a) the fibres lay parallel and perpendicular or (b) at an angle of $\pm 45°$ to the direction of the shear displacement. In case (a) all perpendicular fibres connect the sheared edges. These fibres will be stressed with increasing shear deformation. In case (b) some fibres are non-load carrying members whereas the others connect the sheared edges. With increasing shear deformation, the membrane behaviour will be dominated by the latter group whereas the first group remains stress-free in this loading case. In Fig. 9, the reaction forces in shear direction are plotted against the linearized strain of the stretched fibres.

In the shear test (a) only one set of fibres is loaded. Therefore the direction of the shear displacement is not important. In case (b), the direction of the shear displacement is changing the result: for the positive shear angle the stiffer fibres are stretched whereas in the opposite case the weaker fibres carry the load. In general, good agreement in all cases is found for moderate strains. Note that no data from shear tests were used to fit the material parameters.

4.4. Reduction to linear elasticity

The motivation behind the use of nine terms in W_{iso}^{+} and W_{ani} was to make the reduction to orthotropic linear elasticity possible. The latter step gives some insight into the physical meaning of certain parameters. Let us require $\mathbf{S}_{\text{iso}}^{+}$ and $\mathbf{S}_{\text{ani}}$ to be linear in $\mathbf{C}$. To achieve this, the exponents must be chosen according to

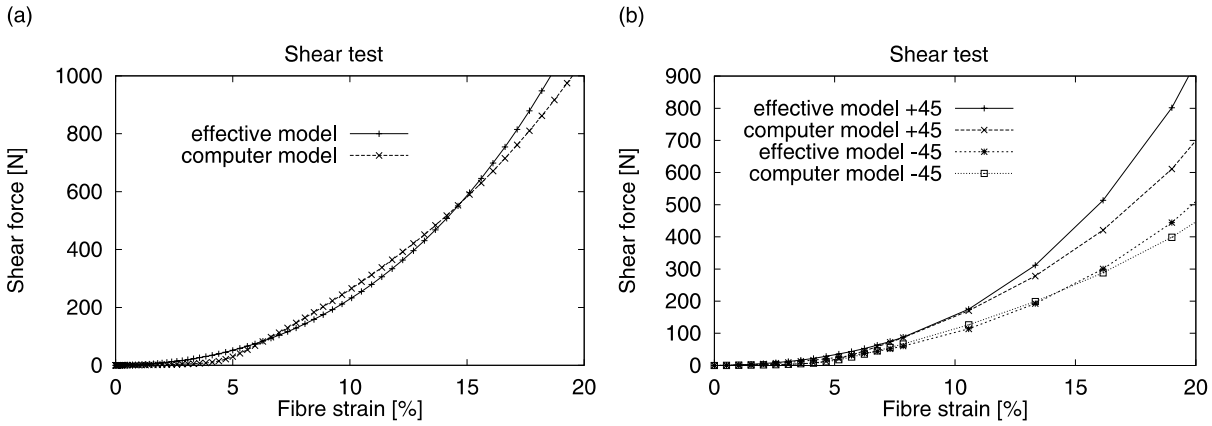

Fig. 9. Force–strain behaviour for shear deformation, different fibre orientations (a) 0/90° and (b) $\pm 45°$.

$$\begin{aligned}
&\alpha_1 = 2, \quad \alpha_2 = 1,\\
&\beta_1 = 2, \quad \beta_2 = 1,\\
&\gamma_1 = 2, \quad \gamma_2 = 1,\\
&\delta_1 = 1, \quad \delta_2 = 1,\\
&\xi = 1.
\end{aligned} \tag{35}$$

Note that in order to obtain a stress-free undeformed state, the terms

$$\Delta W_{\text{iso}}^{+} = -2K_2^{\text{iso}}(I_1 - 3) \quad \text{and} \quad \Delta W_{\text{ani}} = -4K_2^{\text{ani}\,1}(I_4 - 1) - 4K_2^{\text{ani}\,2}(I_6 - 1) \tag{36}$$

must be added to the strain energy function. Finally, the linear model reads

$$\begin{aligned}
W_{\text{lin}} = {} & K_1^{\text{iso}}(I_1 - 3)^2 + K_2^{\text{iso}}(I_2 - 3 - 2(I_1 - 3)) + K_1^{\text{ani}\,1}(I_4 - 1)^2 + K_2^{\text{ani}\,1}(I_5 - 1 - 4(I_4 - 1))\\
& + K_1^{\text{ani}\,2}(I_6 - 1)^2 + K_2^{\text{ani}\,2}(I_7 - 1 - 4(I_6 - 1)) + K^{\text{coup}\,1}(I_1 - 3)(I_4 - 1) + K^{\text{coup}\,2}(I_1 - 3)(I_6 - 1)\\
& + K^{\text{coup ani}}(I_4 - 1)(I_6 - 1).
\end{aligned} \tag{37}$$

The second Piola–Kirchhoff stress tensor is given by

$$\mathbf{S}_{\text{lin}} = \frac{\partial W_{\text{lin}}}{\partial \mathbf{E}} = \mathscr{L}_{\text{lin}} : \mathbf{E}, \tag{38}$$

where $\mathbf{E} = 1/2(\mathbf{C} - \mathbf{1})$ denotes the Green–Lagrange strain tensor. Utilizing the equations

$$\begin{aligned}
&\tfrac{1}{2}((\text{tr}\mathbf{E})^2 - \text{tr}\mathbf{E}^2) = \tfrac{1}{4}(I_2 - 3 - 2(I_1 - 3)),\\
&\text{tr}(\mathbf{E}^2 \cdot \mathbf{M}_1) = \tfrac{1}{4}(I_5 - 1 - 2(I_4 - 1)),\\
&\text{tr}(\mathbf{E}^2 \cdot \mathbf{M}_2) = \tfrac{1}{4}(I_7 - 1 - 2(I_6 - 1)),
\end{aligned} \tag{39}$$

the constant material tensor $\mathscr{L}_{\text{lin}}$ is calculated with

$$\begin{aligned}
\mathscr{L}_{\text{lin}} = {} & (8K_1^{\text{iso}} + 4K_2^{\text{iso}})\mathbf{1} \otimes \mathbf{1} - 4K_1^{\text{iso}}\mathscr{I} + 8K_1^{\text{ani}\,1}(\mathbf{M}_1 \otimes \mathbf{M}_1) + 4K_2^{\text{ani}\,1}\mathscr{E}_1 + 8K_1^{\text{ani}\,2}(\mathbf{M}_2 \otimes \mathbf{M}_2)\\
& + 4K_2^{\text{ani}\,2}\mathscr{E}_2 + 4K^{\text{coup}\,1}(\mathbf{1} \otimes \mathbf{M}_1 + \mathbf{M}_1 \otimes \mathbf{1}) + 4K^{\text{coup}\,2}(\mathbf{1} \otimes \mathbf{M}_2 + \mathbf{M}_2 \otimes \mathbf{1})\\
& + 4K^{\text{coup ani}}(\mathbf{M}_1 \otimes \mathbf{M}_2 + \mathbf{M}_2 \otimes \mathbf{M}_1).
\end{aligned} \tag{40}$$

The coefficients of the fourth-order tensors $\mathscr{E}_1$ and $\mathscr{E}_2$ are given by

$$(E_1)_{ijkl} = (M_1)_{ik}\delta_{jl} + (M_1)_{jk}\delta_{il} \quad \text{and} \quad (E_2)_{ijkl} = (M_2)_{ik}\delta_{jl} + (M_2)_{jk}\delta_{il}. \tag{41}$$

The linear orthotropic model includes only nine constants. In the case of transverse isotropy ($\mathbf{M}_1 = \mathbf{M}$, $\mathbf{M}_2 = \mathbf{0}$), this number reduces further to 5 (see also standard text books like Spencer (1984), Jones (1999)). Using $\mathbf{n}_1^T = \{1, 0, 0\}$, the Voigt matrix representation of the material tensor $\mathscr{L}_{\text{lin}}$ takes the form (subscript lin omitted)

$$\mathscr{L} = \begin{bmatrix} \mathscr{L}_{\text{stretch}}^{3\times 3} & 0 \\ 0 & \mathscr{L}_{\text{shear}}^{3\times 3} \end{bmatrix} \tag{42}$$

with

$$\mathcal{L}^{3\times3}_{\text{stretch}} = \left[\begin{array}{c|c|c} 8K_1^{\text{iso}} & 8K_1^{\text{iso}} & 8K_1^{\text{iso}} \\ & +4K_2^{\text{iso}} & +4K_2^{\text{iso}} \\ +8K_1^{\text{ani}\,1} & & \\ +8K_2^{\text{ani}\,1} & & \\ +8K^{\text{coup}\,1} & +4K^{\text{coup}\,1} & +4K^{\text{coup}\,1} \\ \hline \text{symm} & 8K_1^{\text{iso}} & 8K_1^{\text{iso}} \\ & & +4K_2^{\text{iso}} \\ \hline \text{symm} & \text{symm} & 8K_1^{\text{iso}} \end{array}\right] \tag{43}$$

and

$$\mathcal{L}^{3\times3}_{\text{shear}} = \left[\begin{array}{c|c|c} -2K_2^{\text{iso}} + 2K_2^{\text{ani}\,1} & 0 & 0 \\ \hline 0 & -2K_2^{\text{iso}} & 0 \\ \hline 0 & 0 & -2K_2^{\text{iso}} + 2K_2^{\text{ani}\,1} \end{array}\right]. \tag{44}$$

The comparison with linear isotropic elasticity yields the relations

$$K_2^{\text{iso}} = -\tfrac{1}{2}\mu \quad \text{and} \quad K_1^{\text{iso}} = \tfrac{1}{8}(\Lambda + 2\mu). \tag{45}$$

The parameters $K_1^{\text{ani}\,1}$ and $K_2^{\text{ani}\,1}$ describe the increased stiffness in fibre direction. Among these, $K_2^{\text{ani}\,1}$ has a meaning somewhat similar to the shear modulus in isotropic elasticity. It enters the shear matrix which is not the case for $K_1^{\text{ani}\,1}$. The parameter $K^{\text{coup}\,1}$ serves to describe the coupling between the strains in 1- and 2- as well as in 1- and 3-direction.

Certainly, the non-linear model is far more complicated. However the considerations made in the context of the linear model are still valid. For instance, look at the parameters $K^{\text{coup}\,i}$ $(i = 1, 2)$ and $K^{\text{coup ani}}$. $K^{\text{coup ani}}$ lies in the range of the rubber stiffness, because the interaction between the fibres in the two directions is only due to the rubber matrix. The other coupling constants $K^{\text{coup}\,i}$ $(i = 1, 2)$ vanish.

5. Finite element formulation

Since pneumatic membranes possess hardly any stiffness in bending or compression, they wrinkle easily. The same effect is observed in every day life for all sorts of clothing made of fabric. The wrinkling represents an instability phenomenon like the buckling of shells and plates and is accompanied by a relatively sudden increase of the displacement in the direction perpendicular to the membrane surface. Certainly, such a behaviour should be avoided in practical applications. In order to investigate the sensitivity of the membrane with respect to wrinkling, we have to include the bending deformation in the finite element formulation. Many authors work therefore with sophisticated shell formulations. See in the context of composites e.g. Dorninger and Rammerstorfer (1990), Gruttmann et al. (1993) and Stein and Teßmer (1998a,b). The coding of such elements is, however, usually elaborate. Moreover, due to the fact that an integration over the thickness of the shell is necessary, the implementation of three-dimensional material laws requires further considerations. For these reasons it is desirable to work with brick formulations, where the continuum mechanical equations can be implemented directly. To use 3D elements for this purpose is only reasonable from the point of view of computational efficiency, if a locking-free formulation is available. An appropriate method has been recently developed by Reese et al. (2000) (see also Reese et al.

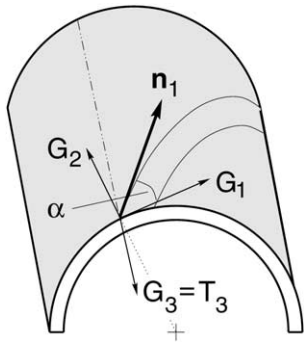

Fig. 10. Cylindrical geometry.

(1999)). The latter formulation is based on the classical concept of reduced integration plus hourglass stabilization (see for small deformations Belytschko et al. (1984)). Exploiting the analogy with the enhanced strain concept in a linearized form, we are able to determine the so-called stabilization factors in such a way that locking-free behaviour is obtained. In this way, we obtain an extremely simple and efficient element which works with only one Gauss point. Note that the calculation of the stabilization factors can be done analytically as soon as the deformed configuration of the element is known.

In the case of curved surfaces, one has to take into account that the vector $\mathbf{n}_1$ tangential to the fibre is not constant. Consequently, we have to compute the structural tensor in each element using information such as the geometry of the structure and the orientation angle α (see for the example of a cylinder geometry Fig. 10).

The covariant basis

$$\mathbf{G}_j = \underbrace{(\mathbf{G}_i \otimes \mathbf{E}_i)}_{:=\mathbf{J}} \cdot \mathbf{E}_j \tag{46}$$

can be easily determined by means of the Jacobi matrix $\mathbf{J} = \partial \mathbf{X}/\partial \boldsymbol{\xi}$ (X^i Cartesian coordinates, ξ^i local (convective) coordinates). We construct a vector

$$\mathbf{T}_3 = -\frac{G_{13}}{G_{11}}\mathbf{G}_1 + \mathbf{G}_3 \tag{47}$$

which fulfils the condition $\mathbf{G}_1 \cdot \mathbf{T}_3 = 0$. Then, $\mathbf{T}_3$ is perpendicular to $\mathbf{G}_1$ and lies in the plane given by $\mathbf{G}_1$ and $\mathbf{G}_3$. The "structural vector" $\mathbf{n}_1$ is calculated using the relationship

$$\mathbf{n}_1 = \cos\alpha \bar{\mathbf{G}}_1 - \sin\alpha \bar{\mathbf{T}}_3, \tag{48}$$

where $\bar{\mathbf{T}}_3 = \mathbf{T}_3/|\mathbf{T}_3|$ and $\bar{\mathbf{G}}_1 = \mathbf{G}_1/|\mathbf{G}_1|$ denote normalized vectors. This procedure is very cheap from the computational point of view and can be carried out for any shell geometry. Note that in the special case of a cylinder, we obtain $G_{13} = 0$ and, as indicated in Fig. 10, $\mathbf{G}_3 = \mathbf{T}_3$.

6. Numerical examples

In this section, two examples are discussed in detail. First, the performance of the present brick element formulation is compared with the one of a classical shell element. In the second example, we investigate the inflation of a flat membrane.

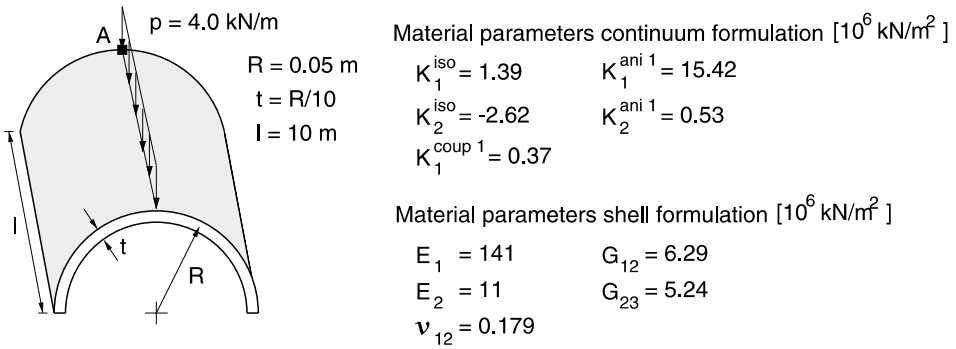

Fig. 11. Pinched cylinder: geometry and material parameters.

6.1. Pinched cylinder

The geometry and the material parameters for this example are given in Fig. 11. The cylinder is clamped at the bottom and consists of unidirectional laminate layers. To carry out a comparison with the shell formulation of Stein and Teßmer (1998a,b) we work here with the transversely isotropic model of linear elasticity presented in Section 4.4. In the 3D calculations, we take one element over the thickness per layer, i.e. one Gauss point in the present element technology. The shell formulation uses also a one Gauss point integration over the thickness and five degrees of freedom per node. Thus, each shell element is associated with 20 degrees of freedom, whereas the brick formulation is based on 24 degrees of freedom.

In Fig. 12a, the vertical displacements for a shell structure with one UDL layer ($\alpha = 30°$) are shown (3D discretization on the left, discretization with shell elements on the right). As a result of the fibre orientation, the displacements are point symmetric. Both the values of the displacement and its distribution agree very well. The same holds for the corresponding stresses in axial direction (Fig. 12b).

In another computation, we assume that the structure shown in Fig. 11 consists of two layers ($\alpha = \pm 30°$). Again, a very good agreement is achieved (see e.g. the stresses in axial direction in Fig. 12c). Note that these stresses are not perfectly symmetric because of the thickness effects. The deviation between the 3D and the shell computation is here larger, since the shell results have been evaluated exactly in the shell midsurface whereas the stress in the left part of Fig. 12c (3D computation) refers to the middle of either the upper or the lower layer.

Finally, the performance of the two element formulations is compared by means of a study of convergence. The displacement in point A (defined in Fig. 11) is plotted against the number of elements (Fig. 13). For the thick cylinder example ($r/t = 10$) the rate of convergence is almost equal. In the case of a thin shell ($r/t = 100$), the shell formulation gives more accurate results for less than 1500 elements. For a discretization with 1800 elements, however, convergence is achieved with both formulations.

6.2. Inflation of a rectangular membrane

The continuum mechanical model (Section 4) was derived on the basis of biaxial and uniaxial tension tests for the flat membrane (10×16 mm, thickness 0.3 mm). In order to build up a pneumatic structure, such membranes are inflated, i.e. exposed to a deformation-dependent pressure loading. The purpose of this example is to investigate whether the present material model yields physically reasonable results also in this case. The material parameters are taken from Eq. 34. In the left half of the system (Fig. 14), the fibres are lying in horizontal and vertical directions ($\alpha = 0°/90°$). In the right half, we have the orientation angles

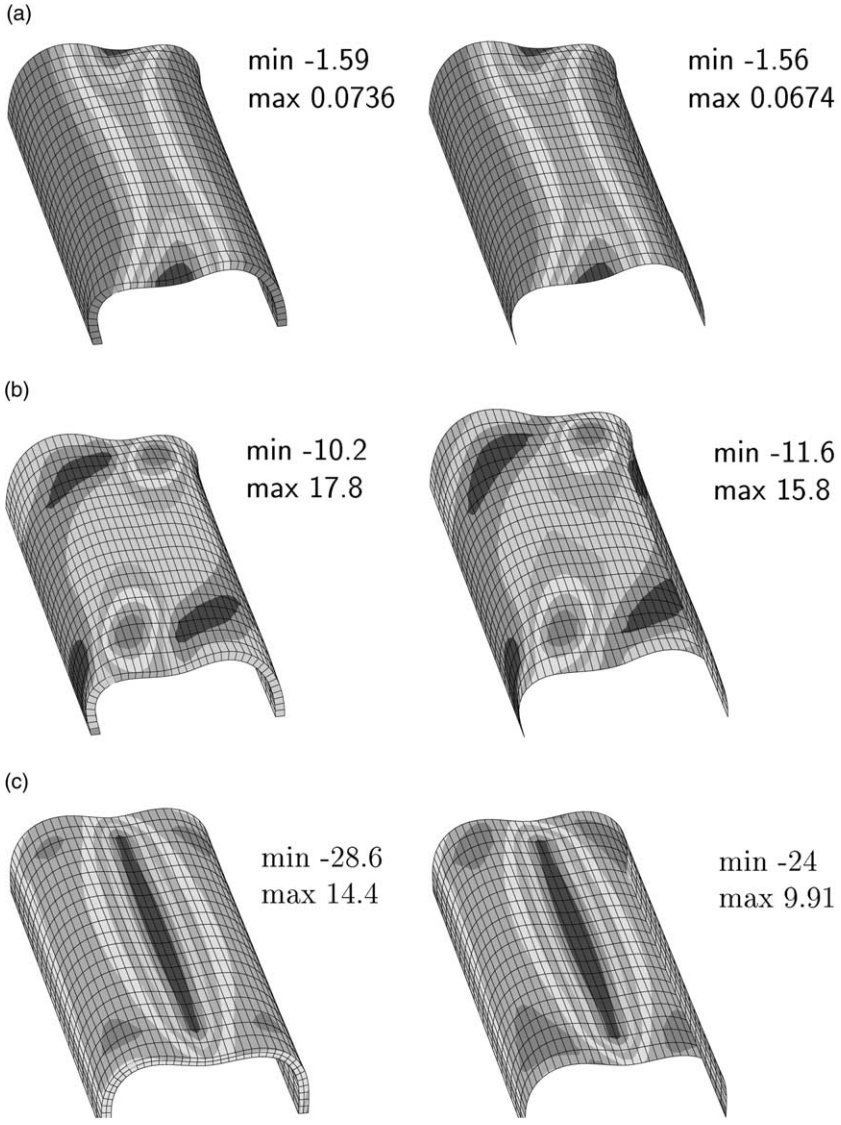

Fig. 12. (a) Vertical displacement (cm), one layer 30°; (b) PK stress in axial direction (kN/cm^2), one layer 30°; (c) PK stress in axial direction (kN/cm^2), two layers $\pm 30°$.

$\alpha = \pm 45°$. Due to the fact that a pneumatic membrane structure usually consists of several pieces sewn together, such discontinuities are characteristic in practical applications.

The boundary conditions are set as follows: all displacements on the outer edges are constrained only on one side of the membrane. It can therefore rotate around the edge without bending constrains. Non-conservative pressure loading is applied as indicated in Fig. 15. See for more details Schweizerhof and Ramm (1984) and Simo et al. (1991). Due to the seam in the middle of the structure, we obtain very different deformation behaviour in the two pieces (see in particular Fig. 16b).

Fig. 16 shows the 11- and 22-components of the left Cauchy–Green tensor $\mathbf{b} = \mathbf{F} \cdot \mathbf{F}^T = b_{ij} \mathbf{e}_i \otimes \mathbf{e}_j$. The 11-component is continuous whereas the corresponding plot for the 2-direction shows a jump at the seam.

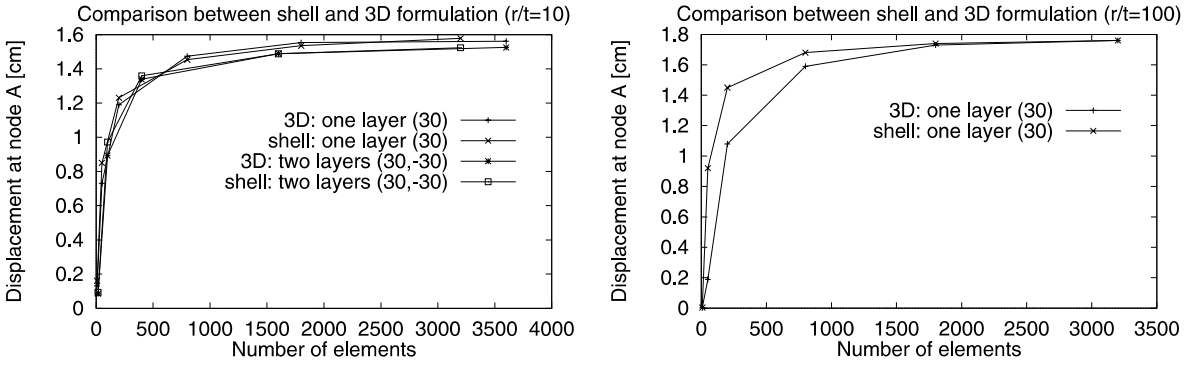

Fig. 13. Convergence behaviour.

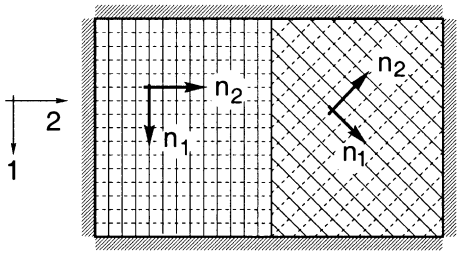

Fig. 14. Rectangular membrane: geometry and boundary conditions.

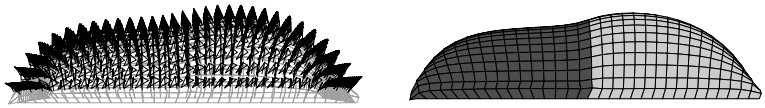

Fig. 15. Loading and deformed geometry.

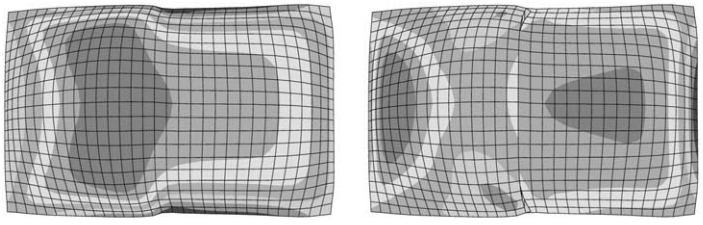

Fig. 16. Strains for the principal directions.

An explanation for this fact can be given quite easily. In 2-direction (long side), we can have different strains on both sides. Only the displacements have to coincide in the interconnection area. In 1-direction (short side), also the strains must be equal, since the material on the left and the right side of the seam cannot

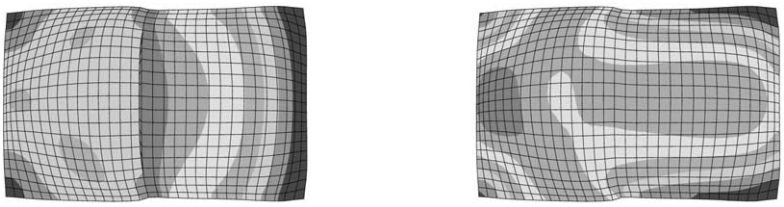

1-direction,
(max 12.2 N/mm^2, min -0.4 N/mm^2)

2-direction,
(max 6.34 N/mm^2, min -0.2 N/mm^2)

Fig. 17. Cauchy stresses.

move relative to each other. For the Cauchy stresses (see Fig. 17), a discontinuity is found for the 1-direction whereas the stress field in 2-direction is smooth. This result can be derived from the local equilibrium condition $\boldsymbol{\sigma}_{\text{left}} \cdot \mathbf{n} = \boldsymbol{\sigma}_{\text{right}} \cdot \mathbf{n}$, $\mathbf{n}$ being the normal vector of the interconnection area.

7. Conclusions

The main goal of this paper has been to model the anisotropically elastic material behaviour of fibre reinforced membranes. It has to be taken into account, that moderate deformations (up to 40%) occur. Unfortunately, experimental results for the stress–strain behaviour are poorly documented in the literature. So we follow a different strategy. Since test results for the fibres alone are more easily accessible, we begin with formulating a one-dimensional model for the fibre deformation. The "1D" material parameters are fitted to the experimental results. As expected, we obtain slightly different values for the warp and the weft thread. Then we set up a finite element discretization, where the fibres are modeled by means of non-linear truss elements and the rubber coating by the Neo-Hooke model implemented into a brick element formulation. Simulating various biaxial and uniaxial experiments with such a "virtual" test piece, we are able to generate sufficient test data. Certainly, these "experimental" results are artificial and cannot replace real data. However the computer data are much cheaper and still serve to develop a physically reasonable model. The material parameters can then be fitted also to real test curves, as soon as these are available. One main advantage is the prediction of response changes due to changes in the fibre direction. As an additional benefit, we gain a deeper understanding of what happens inside the material.

Of crucial importance is to take into account that the fibres behave differently in tension and compression. For this purpose, we check the values of the invariants and "switch-off" certain material parameters accordingly. In this way, we differentiate between orthotropic (biaxial tension), transversely isotropic (uniaxial tension or compression) and isotropic material behaviour (biaxial compression). In order to guarantee the stability of the material law, further restrictions have to be introduced.

The results are promising and are in astonishingly good agreement for all five tests. The model includes 15 material parameters. Considering the complexity of the present material behaviour, this is an appropriate number. To control the fit, we carry out two independent shear tests. Agreement is achieved up to 15–20% fibre strain. Note that we do not use the shear tests to fit the material parameters.

The implementation of the material model into a finite element code is straightforward, if one works with a brick element formulation. To attain satisfactory computational efficiency, a special element technology is necessary. Here, we work with the stabilization technique recently developed by Reese et al. (2000). The comparison with a classical shell formulation shows that the 3D element yields a comparable performance. Geometry-dependent structural tensors can be incorporated easily. Further developments should focus in particular on inelastic effects and deformation-induced anisotropy.

Acknowledgements

The authors thank Jan Teßmer for the calculation of the shell examples and useful discussions on important aspects of this work. Further we gratefully acknowledge the support of the Deutsche Forschungsgemeinschaft (DFG) under project Wr 19/16-1.

References

Ball, J.M., 1977. Convexity conditions and existence theorems in nonlinear elasticity. Archive for Rational Mechanics and Analysis 63, 337–403.

Belytschko, T., Ong, J.S.-J., Liu, W.K., Kennedy, J., 1984. Hourglass control in linear and nonlinear problems. Computer Methods in Applied Mechanics and Engineering 43, 251–276.

Bidmon, W., 1989. Zum Weiterreißverhalten von beschichteten Geweben, Dissertation, Fachbereich Bauingenieur-und Vermessungswesen, Universität Stuttgart.

Boehler, J.P., 1977. On irreducible representations for isotropic functions. Zeitschrift für Angewandte Mathematik und Mechanik 57, 323–327.

Boehler, J.P., 1979. A simple derivation of representations for non-polynomial constitutive equations in some cases of anisotropy. Zeitschrift für Angewandte Mathematik und Mechanik 59, 157–167.

Bonet, J., Burton, A.J., 1998. A simple orthotropic, transversely isotropic hyperelastic constitutive equation for large strain computations. Computer Methods in Applied Mechanics and Engineering 162, 151–164.

Dorninger, K., Rammerstorfer, F.G., 1990. A layered composite shell element for elastic and thermoelastic stress and stability analysis at large deformations. International Journal for Numerical Methods in Engineering 30, 833–858.

Gruttmann, F., Wagner, W., Meyer, L., Wriggers, P., 1993. A nonlinear composite shell element with continuous interlaminar shear stresses. Computational Mechanics 13, 175–188.

Holzapfel, G.A., Eberlein, R., Wriggers, P., Weizsäcker, H.W., 1996. A new axisymmetrical membrane element for anisotropic, finite strain analysis of arteries. Communications in Numerical Methods in Engineering 12, 507–517.

Jones, M.J., 1999. Mechanics of Composite Materials, second ed. Taylor and Francis, London.

Liu, S., 1982. On representations of anisotropic invariants. International Journal of Engineering Science 20, 1099–1109.

Marsden, J.E., Hughes, T.J.R., 1983. Mathematical foundations of elasticity. Prentice-Hall, Englewood Cliffs.

Ogden, R.W., 1972. Large deformation isotropic elasticity-on the correlation of theory and experiment for incompressible rubberlike solids. Proceedings of the Royal Society of London, Series A 326, pp. 565–584.

Reese, S., Küssner, M., Reddy, B.D., 1999. A new stabilization technique for finite elements in non-linear elasticity. International Journal for Numerical Methods in Engineering 44, 1617–1652.

Reese, S., Wriggers, P., Reddy, B.D., 2000. A new locking-free brick element technique for large deformation problems in elasticity. Computers and Structures 75, 291–304.

Rüter, M., Stein, E., 1999. Analysis, finite element computation and error estimation in transversal isotropic nearly incompressible finite elasticity, Computer Methods in Applied Mechanics and Engineering 190, 519–541.

Schweizerhof, K., Ramm, E., 1984. Displacement dependent pressure loads in nonlinear finite element analysis. Computers and Structures 18, 1099–1114.

Simo, J.C., Taylor, R.L., Wriggers, P., 1991. A note on finite element implementation of pressure boundary loading. Communications in Numerical Methods in Engineering 7, 513–525.

Spencer, A.J.M., 1984. Continuum Theory of the Mechanics of fibre-reinforced Composites. CISM Course and Lectures no. 282, International Center for Mechanical Science, Springer, New York.

Stein, E., Teßmer, J., 1998a. Modelling of delamination progress in multilayered composites by energy release rates. Zeitschrift für Angewandte Mathematik und Mechanik 78 (Suppl. 1), 65–68.

Stein, E., Teßmer, J., 1998b. Theory and Computation of Multilayered Composites. NATO ASI on Mechanics of Composite Materials and Structures, vol. II, pp. 39–48.

Svendsen, B., 1994. On the representation of constitutive relations using structure tensors. International Journal of Engineering Science 32, 1889–1892.

Weiss, J.A., Maker, B.N., Govindjee, S., 1996. Finite element implementation of incompressible, transversely isotropic hyperelasticity. Computer Methods in Applied Mechanics and Engineering 135, 107–128.

Zhang, Q.-S., Rychlewski, J.M., 1990. Structural tensors for anisotropic solids. Archives of Mechanics 42, 267–277.